Synthesis of Carbonate-intercalated Copper–Cobalt Layered Double Hydroxide for Efficient Electrochemical Conversion of 5-Hydroxymethylfurfural into 2,5-Furandicarboxylic Acid

Ayu Sri Wahyuni[1,a], Muthumariappan Akilarasan[3,a], Wasif Farooq[3,4], Mohammed T. Abdullahi,[1] Majad Khan[1,2] Maryum Ali[1,2], Muhammad Nawaz Tahir*[1,2]

[1]*Chemistry Department, King Fahd University of Petroleum & Minerals, Dhahran 31261, Kingdom of Saudi Arabia*

[2]*Interdisciplinary Research Center for Hydrogen Technologies and Carbon Management (IRC-HTCM), King Fahd University of Petroleum & Minerals, Dhahran 31261, Kingdom of Saudi Arabia.*

[3]*Interdisciplinary Research Centre for Refining and Advanced Chemicals (IRC-RAC), King Fahd University of Petroleum & Minerals, Dhahran 31261, Kingdom of Saudi Arabia.*

[4]*Department of Chemical Engineering, King Fahd University of Petroleum & Minerals, Dhahran 31261, Kingdom of Saudi Arabia.*

*Corresponding author: *Muhammad Nawaz Tahir;* muhammad.tahir@kfupm.edu.sa

[a] authors contributed equally.

S1. Product analysis:

The HMF conversion, FDCA yield, and faradaic efficiency were calculated using equations I, II and III, respectively.

$$\text{HMF conversion (\%)} = [n(\text{HMF consumed}) / n(\text{HMF initial})] \times 100 \quad \text{I}$$

$$\text{FDCA yield (\%)} = [n(\text{FDCA formed}) / n(\text{HMF initial})] \times 100 \quad \text{II}$$

$$\text{Faradaic efficiency (\%)} = [n(\text{FDCA formed}) / (\text{Charge} / (6 \times F))] \times 100 \quad \text{III}$$

where F is the Faraday constant (96,485 C mol^{-1}) and n is the mol of reactant calculated from the concentration measured by HPLC. Charge passed 102.3 C.

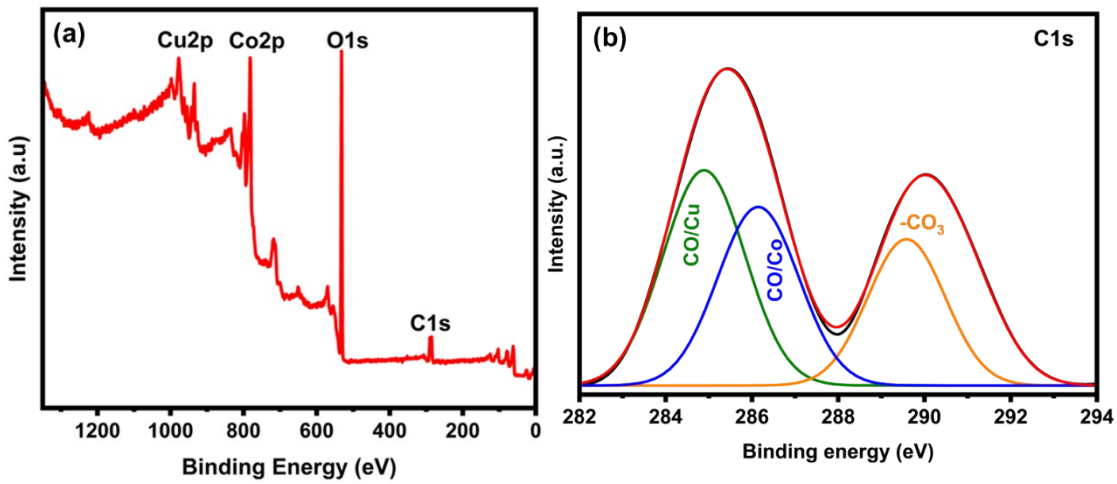

Fig. S1.(a) X-ray Photoelectron Spectroscopy (XPS) survey spectra of all elements. (b) XPS spectrum of the C 1s region for the synthesized CuCo–CO_3 LDH material.

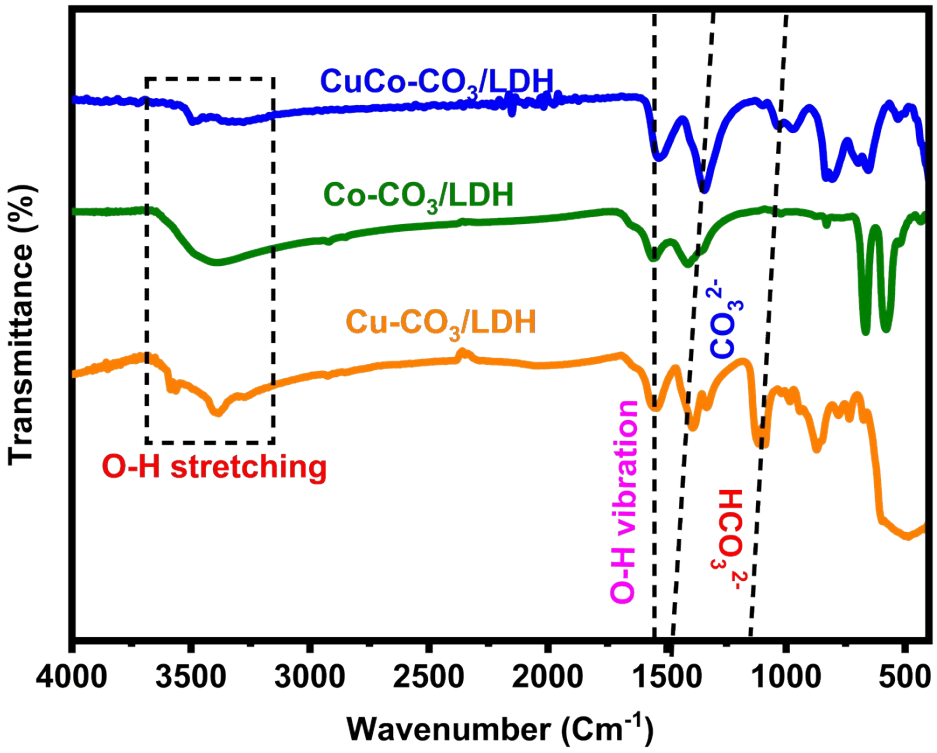

Fig. S2. FTIR spectra of Cu–CO_3/LDH, Co–CO_3/LDH, and CuCo–CO_3/LDH recorded in the range of 4000–400 cm^{-1}.

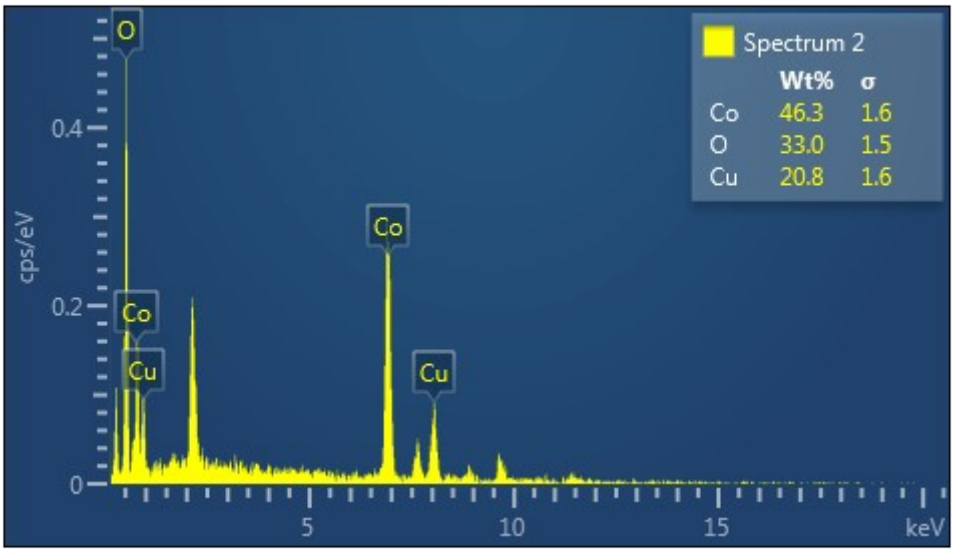

Fig. S3. Energy Dispersive X-ray (EDX) analysis spectrum of CuCo-CO_3/LDH

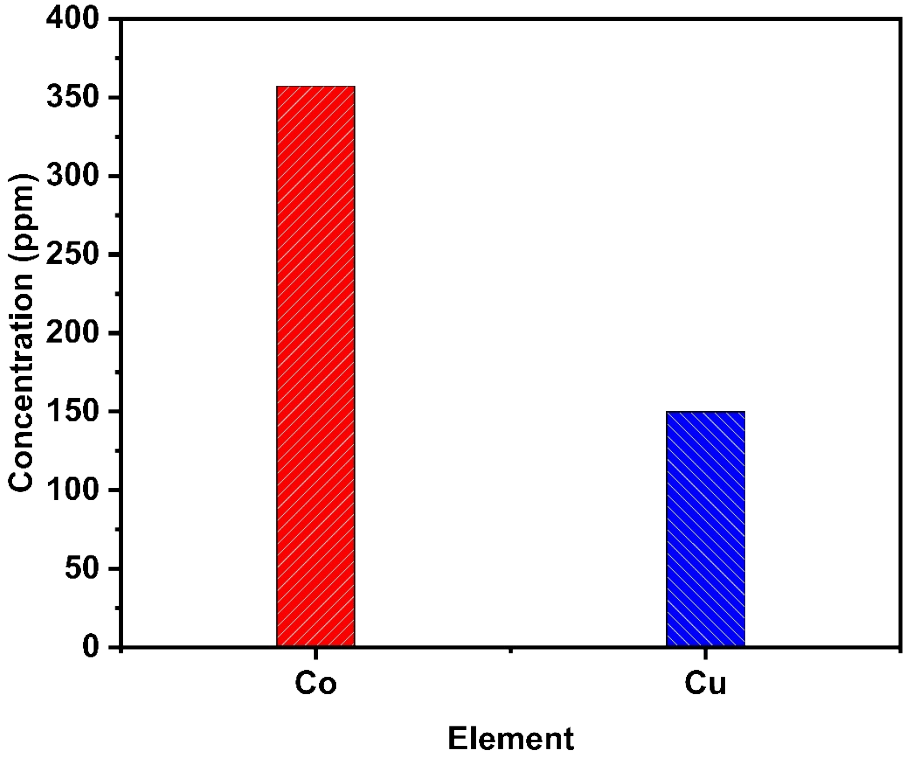

Fig. S4. ICP-OES of CuCo-CO_3-LDH shows the Co and Cu concentration of 357 and 150 ppm.

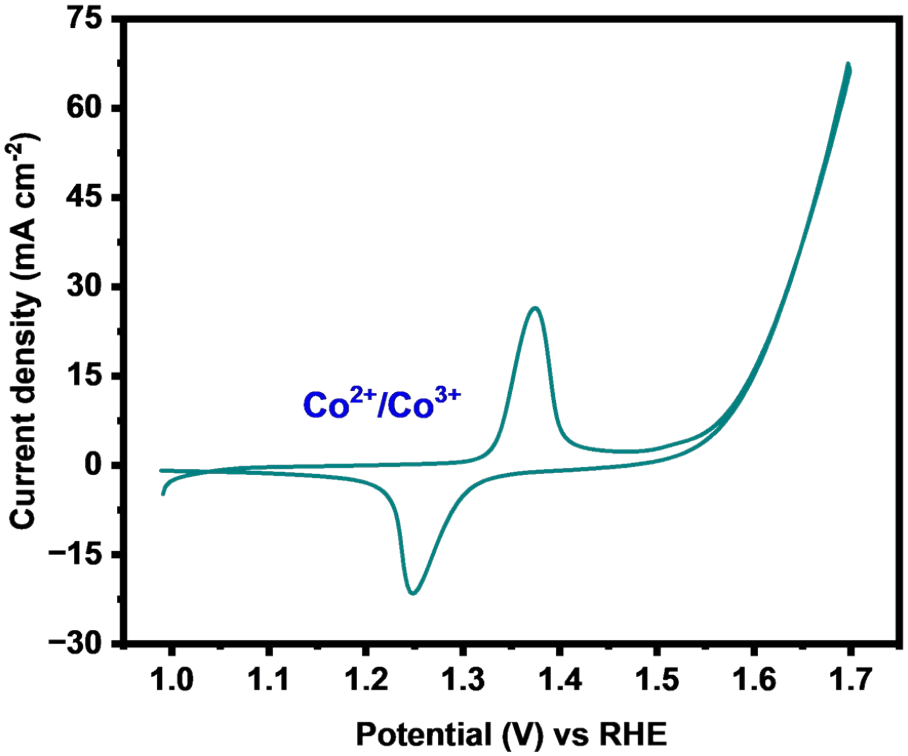

Fig. S5. Cyclic voltammetry (CV) of as-prepared CuCo-CO_3-LDH in 1.0 M KOH with a potential window from 1.0 V to 1.7 V vs. RHE at a scan rate of 5 mV s^{-1}

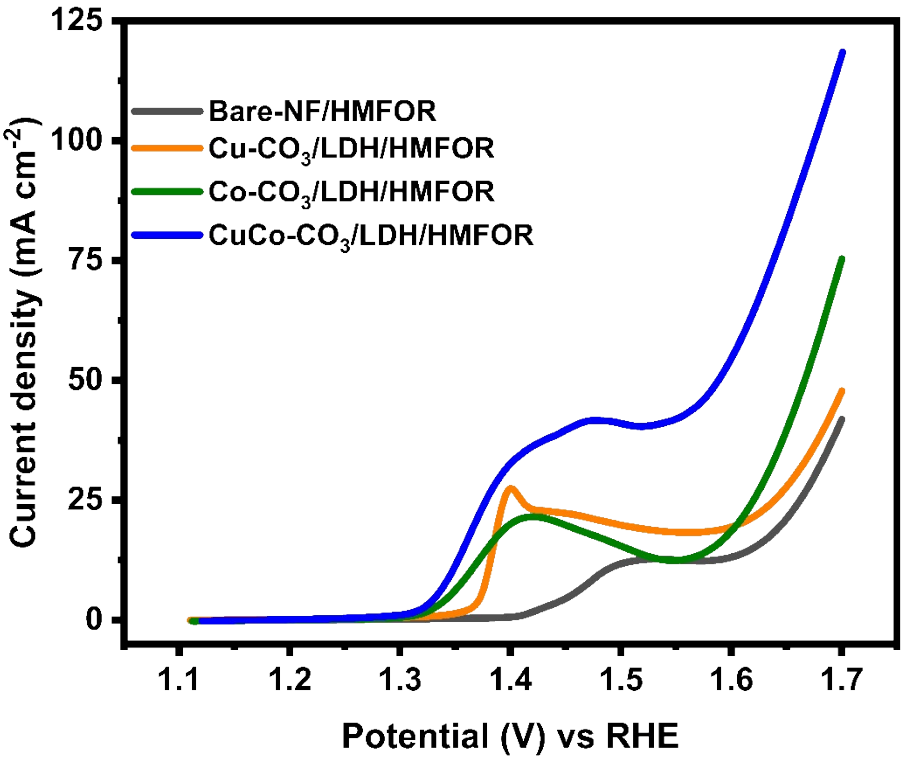

Fig. S6. Comparative linear sweep voltammetry (LSV) curves of bare Ni foam (NF), Cu–CO_3/LDH, Co–CO_3/LDH, and CuCo–CO_3/LDH recorded in 1.0 M KOH containing 10 mM HMF at a scan rate of 5 mV s^{-1}, highlighting the enhanced HMFOR activity and lower overpotential of the CuCo–CO_3/LDH electrocatalyst.

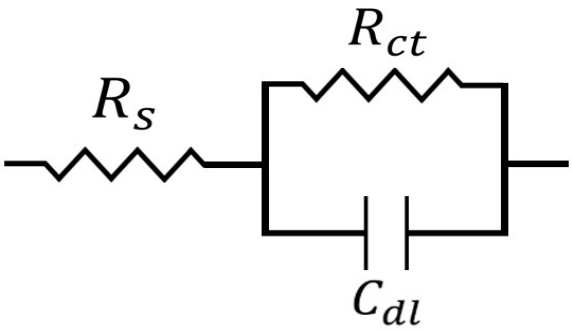

Fig. S7. Randles circuit for EIS fitting model

A simple Randles cell model equivalent circuit was used to analyze the impedance spectra, which include the charge transfer resistance (R_{ct}), solution/series resistance (R_s), and the capacitance of the electrochemical double-layer (C_{dl}).

S6. TOF measurements

The turnover frequency (TOF) for HMFOR can be determined using the equation:

$$TOF=Current/nF\times mol\ active\ sites$$

where F represents Faraday's constant, n is the number of electrons involved in the reaction (6 for HMFOR), and the current is measured at 1.36 V. To calculate the number of active sites, we assume that the observed redox process involves a one-electron transfer, with the Ni redox wave accounting for all electrochemically accessible Ni atoms. The number of active sites can be calculated as:

$$mol\ active\ sites=Q/e\times N_A$$

where Q is the charge associated with the redox process, e is the elementary charge (1.602×10^{-19} C), and N_A is Avogadro's number (6.02×10^{23} mol^{-1}).

S7. Equation for Exchange Current Density (j_0) from Tafel Plot

The Tafel equation is:

$$\eta=blog(j)+a$$

Where, η = overpotential (V), j = current density (A/cm^2), b= Tafel slope (V/decade) and a = intercept constant.

S8. Rate constant calculation

Rate constant can be calculated by Equation,

$$k=\frac{ln(\frac{cf}{ci})}{-(tf-ti)}$$

where c_i and c_f are initial and final concentrations at the different times. t_i and t_f are the initial and final reaction times. The natural log of HMF concentration is plotted against time. The slope of the line is given as -k. Origin Pro Software was employed to perform the kinetic fittings and regression analysis.

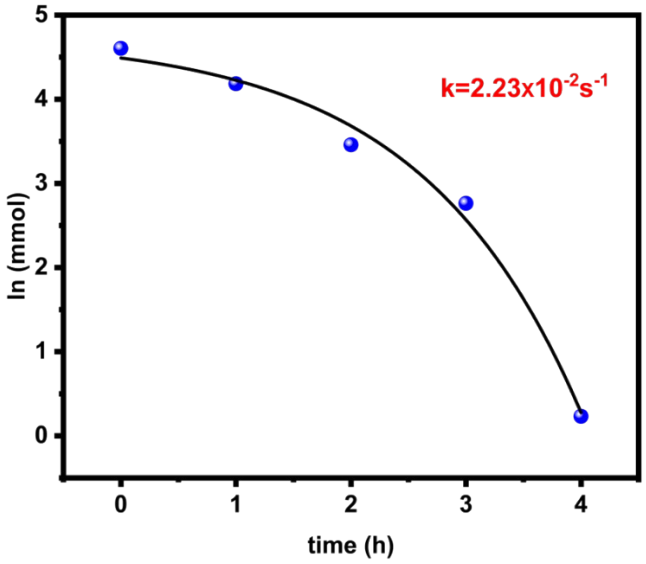

Fig. S8. Estimation of the apparent rate constant for HMF oxidation based on pseudo-first-order kinetics from HPLC data.

Table S1. Comparison of the electrochemical oxidation of HMF to FDCA using CuCo–CO_3/LDH with representative non-electrochemical catalytic oxidation methods, summarizing key parameters such as reaction conditions, HMF conversion, FDCA yield, selectivity, and efficiency.

Process	**Catalyst**	**[HMF]**	**Conditions**	**FDCA Yield**	**Ref.**
Electrochemical	CuCo-LDH/NF	10 mM	1.0 KOH, 4h	97.46%	This work
Photocatalytic	CoPz/g-C_3N_4	10 mM	25 °C, 400 nm LED light, Air atm, 24 h	81%	[1]
Thermal Catalytic	Co–Mn oxide	100 mM	120 °C, 1 MPa O_2, 5 h	95%	[2]
Thermal Catalytic	Ru/NaY zeolite	90 mM	120 °C, 1 MPa O_2, base free, 8 h	94%	[3]
Thermal Catalytic	Pt/CeO_2–La	100 mM	120 °C, 1 MPa O_2, *in situ* base, 10 h	99.6%	[4]

Process	**Catalyst**	**[HMF]**	**Conditions**	**FDCA Yield**	**Ref.**
Electrochemical	CuCo-LDH/NF	10 mM	1.0 KOH, 4h	97.46%	This work
Biocatalytic	Engineered bacteria *P. putida S12*	50 mM	24 h	86%	[5]
Photocatalytic	FePc/Au–TiO_2	20 mM	Photocatalytic conditions with O_2, base	97%	[6]
Thermal Catalytic	Au on hydrotalcite	50 mM	120 °C, ~1.0 MPa O_2, 12–24 h	~100%	[7]
Thermal Catalytic	Au/Al_2O_3	80 mM	70 °C, 1 MPa O_2, 4 h	90%	[8]
Thermal Catalytic	RuOx/MnOx–VC	50 mM	120 °C, 1 MPa O_2, 6 h	86%	[9]
Thermal Catalytic	Ru/MgO	2 mM	90 psi, 160 °C, 4 h	90%	[10]

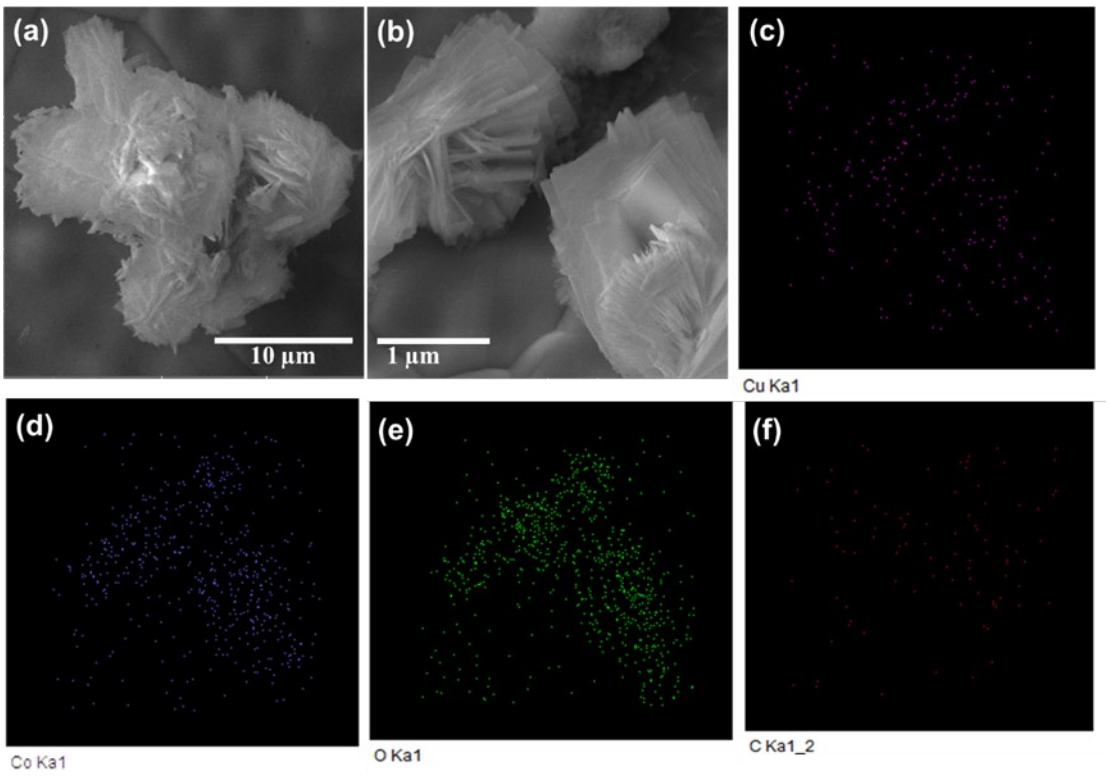

Fig. S9. Post-stability structural characterization of CuCo–CO_3/LDH after electrochemical testing: (a,b) SEM images showing the retained sheet-like morphology with slight aggregation; (c–f) corresponding elemental mapping images of Cu, Co, O, and C, confirming the uniform distribution of active species after long-term electrochemical operation.

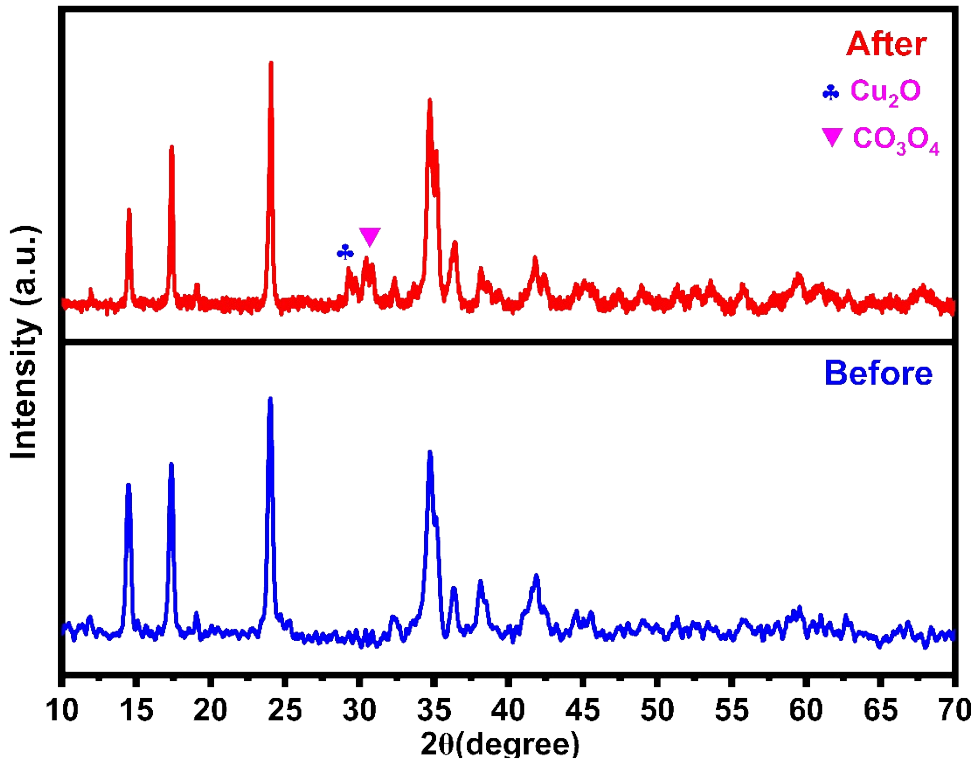

Fig. S10. XRD patterns of CuCo–CO_3/LDH before and after electrochemical stability testing.

References

1 S. Xu, P. Zhou, Z. Zhang, C. Yang, B. Zhang, K. Deng, S. Bottle and H. Zhu, *J Am Chem Soc*, 2017, 139, 14775–14782.

2 K. T. V. Rao, J. L. Rogers, S. Souzanchi, L. Dessbesell, M. B. Ray and C. Xu, *ChemSusChem*, 2018, 11, 3323–3334.

3 P. Kandasamy, P. Gogoi, A. T. Venugopalan and T. Raja, *Catal Today*, 2021, 375, 145–154.

4 W. Yang, H. Yu, B. Wang, X. Wang, H. Zhang, D. Lei, L.-L. Lou, K. Yu and S. Liu, *ACS Appl Mater Interfaces*, 2022, 14, 37667–37680.

5 N. N. Pham, C.-Y. Chen, H. Li, M. T. T. Nguyen, P. K. P. Nguyen, S.-L. Tsai, J.-Y. Chou, T. C. Ramli and Y.-C. Hu, *ACS Synth Biol*, 2020, 9, 1138–1149.

6 L. Li, Y. Wang, Y. Ruan, T. Xu, S. Wu and W. Lu, *Appl Surf Sci*, 2024, 672, 160771.

7 A. Bueno, N. Viar, M. B. Conway, I. Gandarias, J. M. Requies and M. Sankar, *Fuel*, 2026, 403, 136088.

8 C. Megías-Sayago, A. Lolli, S. Ivanova, S. Albonetti, F. Cavani and J. A. Odriozola, *Catal Today*, 2019, 333, 169–175.

9 J. Wu, W. Xie, Y. Zhang, X. Ke, T. Li, H. Fang, Y. Sun, X. Zeng, L. Lin and X. Tang, *Journal of Energy Chemistry*, 2024, 95, 670–683.

10 C. A. Antonyraj, N. T. T. Huynh, K. W. Lee, Y. J. Kim, S. Shin, J. S. Shin and J. K. Cho, *Journal of Chemical Sciences*, 2018, 130, 156.